Conductance fluctuations of monolayer $GeSnH_2$ in the topological phase using a low-energy effective tight-binding Hamiltonian

Zahra Aslani,[1] Esmaeil Taghizadeh Sisakht,[1,2] Farhad Fazileh,[1,*] H. Ghorbanfekr-Kalashami,[2] and F. M. Peeters[2]
[1]*Department of Physics, Isfahan University of Technology, Isfahan 84156-83111, Iran*
[2]*Department of Physics, University of Antwerp, Groenenborgerlaan 171, B-2020 Antwerpen, Belgium*

(Received 10 September 2018; published 15 March 2019)

An effective tight-binding (TB) Hamiltonian for monolayer $GeSnH_2$ is constructed which has an inversion-asymmetric honeycomb structure. The low-energy band structure of our TB model agrees very well with previous *ab initio* calculations even under biaxial tensile strain. Our model predicts a phase transition at 7.5% biaxial tensile strain in agreement with DFT calculations. Upon 8.5% strain the system exhibits a band gap of 134 meV, suitable for room temperature applications. It is shown that an external applied magnetic field produces a special phase which is a combination of the quantum Hall (QH) and quantum spin Hall (QSH) phases; and at a critical magnetic field strength the QSH phase completely disappears. The topological nature of the phase transition is confirmed from: (1) the calculation of the $\mathbb{Z}_2$ topological invariant, and (2) quantum transport properties of disordered $GeSnH_2$ nanoribbons which allows us to determine the universality class of the conductance fluctuations. The application of an external applied magnetic field reduces the conductance fluctuations by a factor of $\sqrt{2}$.

DOI: 10.1103/PhysRevB.99.115421

I. INTRODUCTION

Topological insulators (TIs) have attracted a lot of attention in condensed matter physics and from the materials science community during the past decade [1–5]. TIs are fascinating states of quantum matter with insulating bulk and topologically protected edge or surface states. In two-dimensional (2D) TIs, also known as quantum spin Hall (QSH) insulators [4], the gapless edge states are topologically protected by time reversal symmetry (TRS) and are spin-polarized conduction channels that are robust against nonmagnetic scattering. They are more robust against backscattering than three-dimensional (3D) TIs, making them better suited for coherent transport related applications, low-power electronics, and quantum computing applications [6].

There are currently only a few 3D TI compounds that are experimentally realized such as Bi_2Se_3, Bi_2Te_3, and Sb_2Te_3 [7]; and only HgTe/CdTe [8] and InAs/GaSb [9] quantum wells have been realized as 2D TIs. Also, due to the very small bulk band gaps (on the order of meV), these 2D exhibit TI only at ultralow temperatures. Therefore, there is a great need to find new 2D TIs with large energy band gaps. Following the advancements in graphene and similar materials, intensive efforts have been devoted to explore 2D group-IV and V honeycomb systems, which can harbor 2D topological phases.

In terms of crystal structure, TIs can be generally divided into inversion-symmetric TIs (ISTIs) and inversion-asymmetric TIs (IATIs). In a previous work we have studied $GeCH_3$ which is an inversion symmetric TI under strain [10]. Inversion asymmetry introduces many additional intriguing properties in TIs such as pyroelectricity, crystalline-surface-dependent topological electronic states, natural topological *p-n* junctions, and topological magnetoelectric effects [11–13]. Therefore, 2D IATI materials that are stable at room temperature would be highly promising candidates for future spintronics and quantum computing applications.

Also, it would be interesting if we could implement such features in group-IV honeycomb systems for the integration of devices that use other carbon-IV honeycomb elements. This would avoid issues such as contact resistances and their integration within the traditional Si or Ge based devices.

An efficient method for the synthesis of suitable 2D nanomaterials with honeycomb structure is chemical functionalization. Hydrogenation and halogenation of the above systems for the realization of topological phases have been extensively explored.

Here we consider $GeSnH_2$, which is an inversion asymmetric hydrogenated bipartite honeycomb system. *Ab initio* calculations have shown that monolayers (ML) of GeSn halides ($GeSnX_2$, X = F, Cl, Br, I) are large band gap 2D TIs with protected edge states forming QSH systems [11]. On the other hand, hydrogenated ML GeSn ($GeSnH_2$) is a normal band insulator which can be transformed into a large band gap topological insulator via appropriate biaxial tensile strain [11].

Here we propose a tight-binding (TB) model for a better understanding of the electronic band structure of $GeSnH_2$ near the Fermi level. The band structure of our TB model is fitted to the *ab initio* results, where we consider both cases with spin-orbit coupling (SOC) and without SOC. Within the linear regime of strain the band gap of our TB model agrees very well with the DFT results [11]. This TB model when including SOC predicts a band inversion at 7.5% biaxial tensile strain in agreement with DFT calculations [11]. We show the topological nature of the phase transition from a calculation of the $\mathbb{Z}_2$

*fazileh@cc.iut.ac.ir

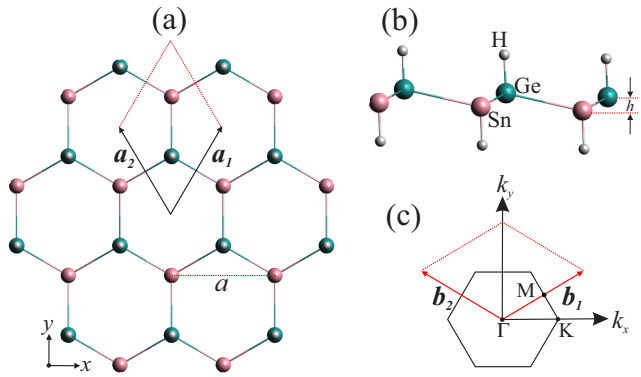

FIG. 1. Top (a) and side (b) views of the ML $GeSnH_2$ structure. $\boldsymbol{a}_1$ and $\boldsymbol{a}_2$ are the lattice vectors, a is the lattice constant, and h is the buckling height. (c) First Brillouin zone of the system with three symmetry points Γ, K, and M and the reciprocal lattice vectors $\boldsymbol{b}_1$ and $\boldsymbol{b}_2$.

topological invariant. When we apply an external magnetic field normal to the plane of the system a QH plus QSH phase appears up to a critical magnetic field strength beyond which the QSH phase completely disappears. Quantum transport of this system is calculated in order to examine the protection of the edge states against nonmagnetic scattering. It is shown that the conductance fluctuations of disordered nanoribbons for energies near the band gap belong to the universality class of the circular unitary ensemble (CUE, $\beta = 2$), while for high energies and strong disorder the fluctuations follow the circular orthogonal ensemble (COE, $\beta = 1$). We found that an applied magnetic field reduces the conductance fluctuations by a factor of $\sqrt{2}$.

This paper is organized as follows. In Sec. II we introduce the crystal structure and lattice constants of monolayer $GeSnH_2$. Our proposed TB model is introduced in the Appendix, and the effect of strain on the electronic properties of $GeSnH_2$ is examined. In Sec. III the topological phase transition under strain is examined by looking at the nanoribbon band structure and by determining the $\mathbb{Z}_2$ topological invariant. The effect of an applied magnetic field is presented in Sec. IV. In Sec. V electronic transport in disordered $GeSnH_2$ nanoribbons is examined and the protection of the chiral edge states against nonmagnetic scatterings is verified. Also, we discuss the universality class of the conductance fluctuations with and without an applied magnetic field. Our results are summarized in Sec. VI.

II. LATTICE STRUCTURE AND TIGHT-BINDING MODEL

The ML $GeSnH_2$ prefers a buckled honeycomb lattice, analogous to its homogeneous counterparts germanene [14] and stanene [15]. Figures 1(a) and 1(b) show the atomic structure of ML $GeSnH_2$ and its geometrical parameters. The 2D honeycomb lattice consists of two inequivalent sublattices made of Ge and Sn atoms, which are named A and B sublattices, respectively. Both Ge and Sn atoms exhibit sp^3 hybridization. One sp^3 orbital is passivated by a hydrogen atom and the other three are bonded to three neighboring Ge or Sn atoms. Thus, the unit cell of $GeSnH_2$ consists of four atoms: one Ge, one Sn, and two hydrogen atoms that are right above (below) the Ge (Sn) atoms. The lattice translation vectors are $\boldsymbol{a}_{1,2} = a(\sqrt{3}/2\hat{y} \pm 1/2\hat{x})$ with the lattice constant $a = 4.41$ Å and the buckling height (h) is 0.76 Å [11,12]. Note that the x and y axes are taken to be along the armchair and zigzag directions, respectively; and the z axis is in the normal direction to the plane of the $GeSnH_2$ film.

Figure 1(c) shows the hexagonal Brillouin zone of ML $GeSnH_2$ with primitive reciprocal lattice vectors $\boldsymbol{b}_{1,2} = 2\pi/a(\sqrt{3}/3\hat{y} \pm \hat{x})$ and three high symmetry points Γ, K, M. The dynamical stability of ML $GeSnH_2$ was previously confirmed by the DFT calculated phonon spectrum [11].

The electronic structure and topological properties of 2D honeycomb ML $GeSnH_2$ were studied in Ref. [11] using first-principle calculations based on DFT. The DFT calculations including spin-orbit interaction predicted that a topological phase transition is induced in ML $GeSnH_2$ through the application of biaxial in-plane tensile strain. It was shown that the low-energy electronic structure of ML $GeSnH_2$ is determined exclusively by using s, p_x, and p_y atomic orbitals of Ge and Sn atoms [11,12]. However, in order to examine the effect of random disorder on the electronic properties of this system and to confirm the topological nature of the phase transition, large system sizes are required. A limitation of the DFT calculations is that only small system sizes are manageable. Therefore, we need to construct a TB model for ML $GeSnH_2$ that is able to describe the low-energy electronic structure of large system sizes.

In the Appendix we derive a low-energy TB model including SOC and we show that the results of the proposed TB model even in the presence of biaxial strain is in very good agreement with previous DFT calculations.

III. TOPOLOGICAL PHASE TRANSITION OF MONOLAYER $GeSnH_2$ UNDER STRAIN

Using our TB model including spin-orbit interaction, we showed that ML $GeSnH_2$ is a NI with a direct band gap of 0.977 eV. We showed that applying biaxial tensile strain modifies its electronic spectrum and a band inversion is taking place at $\epsilon = 7.5\%$.

One way to show that there is a topological phase transition at the critical strain of $\epsilon = 7.5\%$, is to perform calculations of the 1D band structure of nanoribbons with zigzag edges in the presence of biaxial tensile strain, and verify the existence of gapless helical edge states. Here we study the edge state energy bands by cutting a 2D film of ML $GeSnH_2$ into nanoribbons. In our calculations, the Sn and Ge atoms at the edges of the nanoribbon are passivated by hydrogen atoms.

The width of a zigzag $GeSnH_2$ nanoribbon (z-$GeSnH_2$-NR) is defined by N, which is the number of zigzag chains across the ribbon width. In order to reduce the interaction between the two edges, the width of the nanoribbons is taken to be at least 10 nm.

We calculated the band structure of the corresponding nanoribbons. Note that the change of the hopping parameters and the on-site energies of the edge Ge or Sn atoms caused by the passivation procedure is negligible. Therefore, we can use the results in Tables II and III of the Appendix for the on-site energies of Ge and Sn atoms and also for the hopping

TABLE I. Numerical values of the on-site energy of hydrogen atoms and the hopping parameters related to the H-Ge and H-Sn bonds. The energy is in units of eV.

$V^{ss}_{\mathrm{H,Ge}}$	$V^{sp}_{\mathrm{H,Ge}}$	$V^{ss}_{\mathrm{H,Sn}}$	$V^{sp}_{\mathrm{H,Sn}}$	$E^{s}_{H_0}$	$E^{s}_{H_1}$
−4.87	2.05	−4.21	3.63	−1.84	−2.40

parameters corresponding to Ge-Sn bonds in unstrained or strained systems. We have two different on-site energies of hydrogen atoms $E^{s}_{H_0}$ and $E^{s}_{H_1}$, which are pertinent to the hydrogen atoms that are introduced to passivate the Ge and Sn atoms on each edge, respectively. We can write the hopping parameters related to the H-Ge and H-Sn bonds as

$$t^{ss}_{\mathrm{H,X}} = V^{ss}_{\mathrm{H,X}},\ t^{sp_y}_{\mathrm{H,X}} = \pm V^{sp}_{\mathrm{H,X}} \quad (\mathrm{X} = \mathrm{Ge, Sn}), \tag{1}$$

where + (−) denotes the lower (upper) H-X edge bonds. The numerical value of the mentioned hopping parameters and on-site energies of the hydrogen atoms can be obtained by a fitting procedure. The results are shown in Table I.

Figures 2(a) and 2(b) show the energy bands of z-$GeSnH_2$-NR with $N = 26$ in the presence of 5% and 8.5% biaxial tensile strains, respectively. Gapless conducting edge bands are seen for strain of $\epsilon = 8.5\%$. This is consistent with our proposal for the topological phase transition at $\epsilon = 7.5\%$.

It is now well established that for all time reversal invariant 2D band insulators a change in the $\mathbb{Z}_2$ topological invariant from zero to one, indicates a topological phase transition from a NI phase to TI. In our previous works [10,16] we successfully used the algorithm of Fukui and Hatsugai [17] to calculate the $\mathbb{Z}_2$ number to characterize the topology of the energy bands. In this work we implemented the same procedure to confirm the existence of two distinct topological phases in ML $GeSnH_2$. We found that the value of $\mathbb{Z}_2$ switches from zero to one at the critical strain of 7.5%, which confirms the topological nature of the phase transition in the electronic properties of ML $GeSnH_2$.

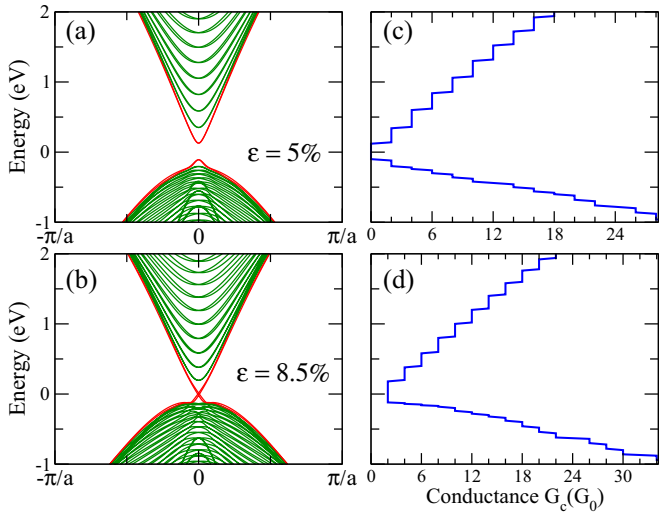

FIG. 2. The 1D energy bands and the total conductance (in units of $G_0 = e^2/h$) of z-$GeSnH_2$-NR for $N = 26$ in the presence of (a) and (c) 5%, (b) and (d) 8.5% biaxial tensile strain.

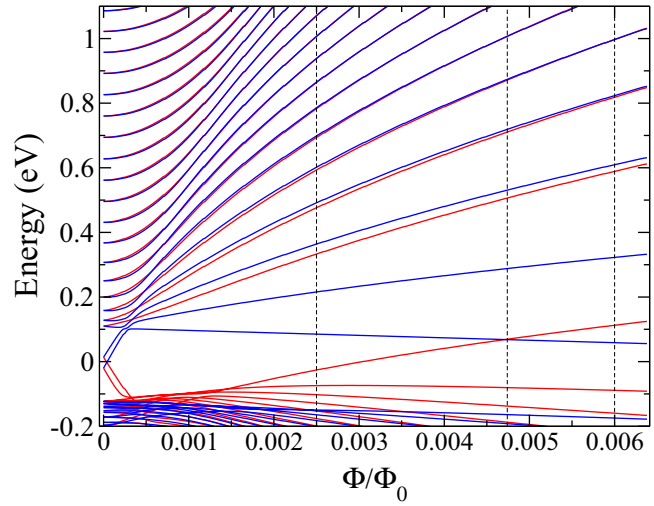

FIG. 3. Landau fan diagrams for a z-$GeSnH_2$-NR of 34 nm width with 8.5% biaxial strain. Φ is the magnetic flux through a honeycomb cell and Φ_0 is the magnetic quantum flux. The band structure of the nanoribbon for the applied magnetic fields at the dashed lines are plotted in Fig. 4. The blue and red bands correspond to opposite spin-polarized states.

IV. THE EFFECT OF AN APPLIED PERPENDICULAR MAGNETIC FIELD

We showed the topological phase transition of ML $GeSnH_2$ under strain using our proposed TB model. Also we confirmed the QSH phase in this system in the presence of biaxial strain by computing the $\mathbb{Z}_2$ invariant and we verified the existence of gapless helical edge states in the z-$GeSnH_2$-NR. These edge states are expected to be protected by TRS. An external magnetic field breaks TRS resulting in the breakdown of the QSH phase [18,19]. In this section we show that the edge states remain robust when an applied magnetic field is turned on and counterpropagating spin-polarized currents exist at both edges (a combination of QSH and QH phases) until a critical field above which the QSH phase completely collapses and there is only one QH phase present.

Here the external magnetic field is modeled by changing the hopping integrals of Eq. (A1) as $t_{i\alpha,j\beta} \rightarrow t_{i\alpha,j\beta}\, e^{-i2\pi\Phi_{i\alpha,j\beta}}$, where $\Phi_{i\alpha,j\beta} = \int_{r_{i\alpha}}^{r_{j\beta}} \mathbf{A}\cdot d\boldsymbol{l}/\Phi_0$, $\Phi_0 = h/e$ denotes the quantum flux, and $\mathbf{A} = (-By,\ 0,\ 0)$ is the vector potential. Due to the small g factor for topological insulators we neglect the Zeeman splitting.

The Landau fan diagram for a zigzag nanoribbon in the presence of strain is plotted in Fig. 3. Here the magnetic flux Φ measures the flux through a honeycomb cell. In Fig. 3 the first crossing point for the edge states at small magnetic fields ($\Phi/\Phi_0 \sim 0.0001$) is a finite size effect corresponding to the overlap of the opposite edge states when the magnetic length approaches the width of the nanoribbon. Therefore, by increasing the ribbon width it moves to zero magnetic field. For higher magnetic fields, as long as the electronlike band (lowest conduction Landau level) is below the holelike band (uppermost valence Landau level), there are counterpropagating spin-polarized states at both edges. In this region the applied magnetic field breaks the balance of the counterpropagating

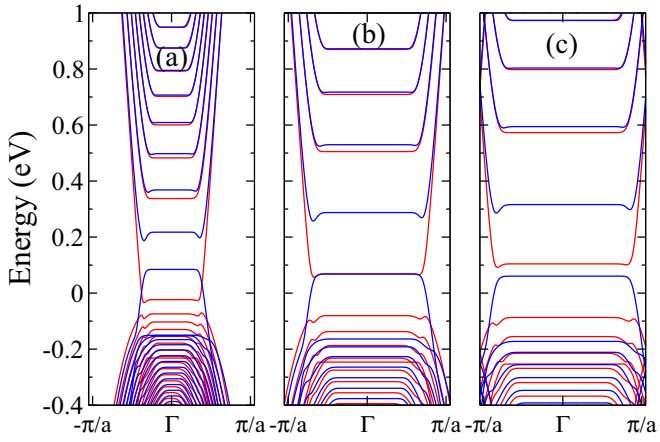

FIG. 4. Landau level band structures of a 34 nm wide zigzag nanoribbon of $GeSnH_2$ with 8.5% biaxial strain for applied perpendicular magnetic fields of (a) $\Phi/\Phi_0 = 0.0025$, (b) $\Phi/\Phi_0 = 0.0047$, and (c) $\Phi/\Phi_0 = 0.006$.

spin-polarized currents at each edge and we have a combination of the QSH and QH phase in the system. For a strong critical magnetic field (the second crossing point for $\Phi/\Phi_0 \sim 0.0047$ is shown in Fig. 3), where the electronlike and holelike bands no longer cross. Now at each edge we have unidirectional currents corresponding to the pure QH phase. After this point the QSH phase is completely removed. In Fig. 4 the Landau level band structure of the system is plotted for three magnetic fields, before, after, and at the critical point. The different colors in this figure correspond to opposite spin polarizations.

V. UNIVERSAL CONDUCTANCE FLUCTUATIONS IN DISORDERED $GeSnH_2$ NANORIBBONS

Transport measurement is a different approach to confirm the existence of helical gapless edge states, which is an important signature of the TI phase. Therefore, we next study the transport properties of ML $GeSnH_2$ nanoribbons in the presence of strain. To this end, we calculate the conductance of z-$GeSnH_2$-NR using the Landauer formalism [20,21]. As is standard the z-$GeSnH_2$-NR is divided into three regions; the left and right leads and the middle scattering region. We initially assume the ribbon to be perfect in order to satisfy the condition of ballistic transport. In the Landauer approach, the total conductance $G_c(E)$ per spin of a nanoscopic device at the Fermi energy (E_F) is given by

$$G_c(E) = \left(\frac{e^2}{h}\right) \mathrm{Tr}\left[\Gamma_L(E) G_D^R(E) \Gamma_R(E) G_D^A(E)\right], \qquad (2)$$

where $\Gamma_{L(R)} = i[\Sigma_{L(R)}(E) - \Sigma_{L(R)}^{\dagger}(E)]$, with $\Sigma_{L(R)}(E)$ being the self-energy of the left (right) lead. $G_D^R(E)$ is the retarded Green's function of the device and $G_D^A(E) = G_D^{R\,\dagger}(E)$. The retarded Green's function of the device is given by

$$G_D^R(E) = \left[E - H_D - \Sigma_L^R(E) - \Sigma_R^R(E)\right]^{-1}. \qquad (3)$$

Here H_D is the Hamiltonian for the device region. The numerically calculated total conductance, in units of $G_0 = e^2/h$, for $N = 26$ as a function of energy is shown in Figs. 2(c) and 2(d) in the presence of 5% and 8.5% biaxial tensile strain, respectively. For strains less than 7.5% ($\epsilon < 7.5\%$), the z-$GeSnH_2$-NR has nonzero conductivity only above a threshold energy corresponding to the minimum energy of the conduction band, which opens a conducting channel with conductance in steps of $2G_0$. As shown in Fig. 2(b), the total conductance at zero energy changes from 0 to 2 by applying biaxial tensile strains larger than 7.5% ($\epsilon > 7.5\%$). The nonzero conductance in the gap originates from the zero energy edge states and also indicates a topological phase transition from NI to TI in ML $GeSnH_2$. These conducting edge states are protected by TRS leading to the robustness of the electronic quantized conductance against backscattering by disorder and therefore holds great promise for spintronics applications [22,23].

It would be helpful to further consider the effect of disorder on the electronic transport properties of this system. The disorder may originate from unwanted dislocations or other defects. Such calculations are another proof for our found strain-induced TI transition. In TIs, the edge states are robust against weak disorder, and only strong disorder can affect the electronic properties.

Here we introduce the disorder in our TB Hamiltonian model $H_{\mathrm{TB}} = H_0 + H_{\mathrm{SOC}}$ using the so-called Anderson disordered model [24] as

$$H_D = \sum_{i,\alpha} W_i c_{i,\alpha}^{\dagger} c_{i,\alpha}, \qquad (4)$$

where W_i is a random number uniformly distributed over the range $[-\frac{W}{2}, \frac{W}{2}]$. We assume a disordered z-$GeSnH_2$-NR with $N = 34$ ($\sim$13 nm width) and 51 nm length as the middle region which is sandwiched between two semi-infinite perfect leads and calculate the conductance averaged over 100 different realizations. The width of the ribbon is chosen large enough in order to avoid finite-size effects. Figure 5(a) shows the average conductance of z-$GeSnH_2$-NR as a function of disorder strength W in the presence of biaxial strain $\epsilon = 8.5\%$ for three different values of the Fermi energy. The energy $E_F = 0.1$ eV corresponds to the energy in the middle of the band gap, while $E_F = 0.35$ eV and $E_F = 1.4$ eV are two energies in the bulk. It can be seen that the averaged quantized conductance at $E_F = 0.1$ eV, which originates from the gapless edge states, is insensitive to weak disorder. The mean conductance decreases only for strong disorder of strength $W > 1.5$ eV which is a signature of a topological insulator.

The universal conductance fluctuations (UCF) [25] are a mesoscopic phenomena, which is caused by the quantum interference of electrons. The UCF are of order e^2/h and correspond to the deviation of the conductance from its ballistic value $G = nG_0$. The standard deviation of conductance in the diffusive regime and zero temperature depends only on the dimensionality and universality class of the disordered mesoscopic system and is independent of the details of the system such as the disorder strength W, the conductance G_c, and the sample size. The UCF takes universal values for three types of symmetry classes corresponding to $\beta = 1$, 2, and 4, respectively. In systems that preserve TRS and spin rotational symmetry (SRS), the symmetry index is $\beta = 1$ (orthogonal ensemble); and $\beta = 2$ corresponds to the case that TRS is

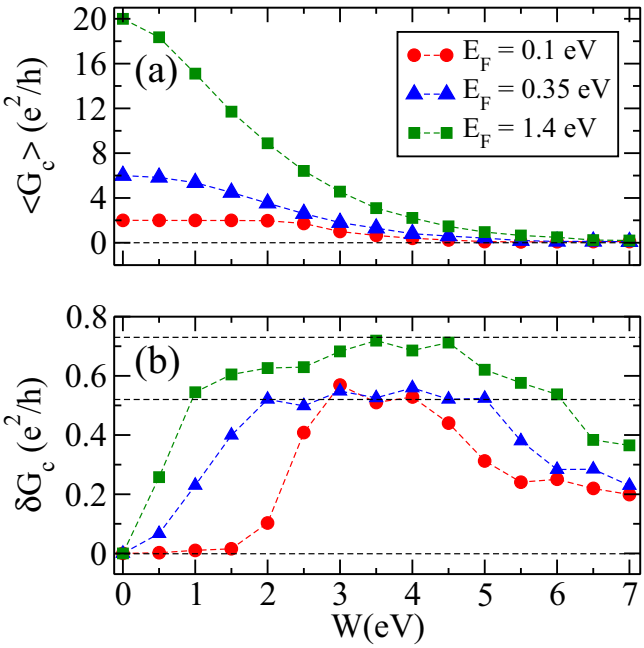

FIG. 5. (a) The mean conductance $\langle G_c \rangle$ and (b) the standard deviation of conductance δG_c of z-GeSnH$_2$-NR with $N = 34$ (13 nm width) and 51 nm length as a function of disorder strength W.

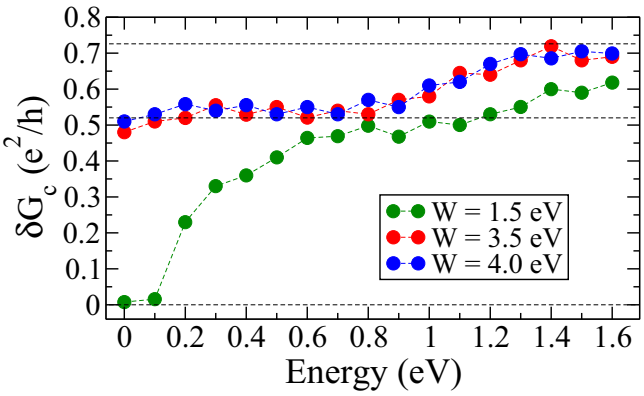

FIG. 6. The standard deviation of conductance δG_c of z-GeSnH$_2$-NR with $N = 34$ and 51 nm length as a function of Fermi energy for three different disorder strengths W = 1.5, 3.5, and 4.0 eV.

broken (unitary ensemble); while $\beta = 4$ is for systems that preserve TRS but with broken SRS (symplectic ensemble) [26,27].

We study numerically the conductance fluctuations in the disordered z-GeSnH$_2$-NR in the presence of biaxial tensile strain. The standard deviation of the conductance $\delta G_c = \langle (G_c - \langle G_c \rangle)^2 \rangle^{1/2}$ of disordered z-GeSnH$_2$-NR is plotted as a function of disorder strength W at three different Fermi energies in Fig. 5(b). There are no conductance fluctuations for energy $E_F = 0.1$ eV in case of weak disorder strength, revealing the robustness of the helical edge states against disorder in the QSH phase. The δG_c approach the value $\sim 0.52\ e^2/h$, which corresponds to the UCF for the symmetry class $\beta = 2$. Our total model Hamiltonian preserves TRS and the reason that the UCF shows the symmetry class $\beta = 2$ is the following: since there are no spin-flip terms (Rashba SOC term) in our model Hamiltonian, we can block diagonal the Hamiltonian matrix with respect to the spin degrees of freedom with zero off-diagonal terms. Then we are dealing with two isolated and identical Hamiltonians corresponding to spin up and spin down states ($H_\uparrow$ and $H_\downarrow$). Each of these blocks lack TRS due to the intrinsic SOC terms, and consequently the total UCF follows the $\beta = 2$ symmetry class. A similar discussion can be found in Refs. [27,28], except that in Ref. [27] spin is not a good quantum number and the Hamiltonian was block diagonalized with respect to the sublattice degrees of freedom.

For high energies and strong disorder strengths, the standard deviation approaches the value $\sim 0.73\ e^2/h$, which belongs to the symmetry class $\beta = 1$. This value can be explained by comparing the localization length with the spin relaxation length (spin relaxation length originates from the intrinsic SOC terms) [29]. As long as the disorder is weak and the localization length is much larger than the spin relaxation length the SOC is significant and the system lacks SRS. But when disorder is strong enough and the localization length is much smaller than the spin relaxation length and when the kinetic energy is much larger than the SOC term (for $E = 1.4$ eV far in the bulk), we can ignore the SOC terms and SRS is preserved and the system follows the $\beta = 1$ symmetry class. Finally, beyond $W \sim 6$ eV, where $\langle G_c \rangle$ approaches the value of $0.3\ e^2/h$ the conductance fluctuations decreases and approaches the superuniversal curve [30] that is independent of dimensionality and symmetry. The superuniversal curve is beyond $W = 7$ eV, which is not shown in Fig. 5.

In Fig. 6 the conductance fluctuations are plotted as a function of the Fermi energy for three disorder strengths. For strong disorder ($W = 3.5$, 4.0 eV), the standard deviation δG_c is around $0.52\ e^2/h$ indicating the unitary ensemble for the conductance fluctuations. The fluctuations approach the value of $\sim 0.73\ e^2/h$ by increasing the Fermi energy as long as the disorder is sufficiently strong and the SOC effects become negligible. The system now follows the orthogonal ensemble. When disorder strength is weak, there is no conductance fluctuations for energies in the gap, confirming the robustness of the helical edge states. The fluctuations increase with increasing disorder. Similarly, they approach the unitary ensemble at the intermediate energies and for higher energies where SOC is negligible and they approach the orthogonal ensemble.

We have also examined the effect of applying an external magnetic field along the $\hat{z}$ direction on the UCF for the disordered z-GeSnH$_2$-NR in the presence of biaxial tensile strain. By applying an external magnetic field to a disordered metal with very weak SOC or without SOC, the universality class changes from COE ($\beta = 1$) to CUE ($\beta = 2$) due to the breaking of TRS.

Figure 7 shows the gradual reduction of the δG_c value from 0.73 to $0.52\ e^2/h$ for $E_F = 1.4$ eV and from 0.52 to $0.365\ e^2/h$ for $E_F = 0.35$ eV by increasing magnetic field. It is shown that by increasing magnetic field which breaks the TRS, the UCF value decreases by a factor of $\sqrt{2}$ in both cases, and it is converged to the reduced value for $\Phi/\Phi_0 > 10^{-3}$.

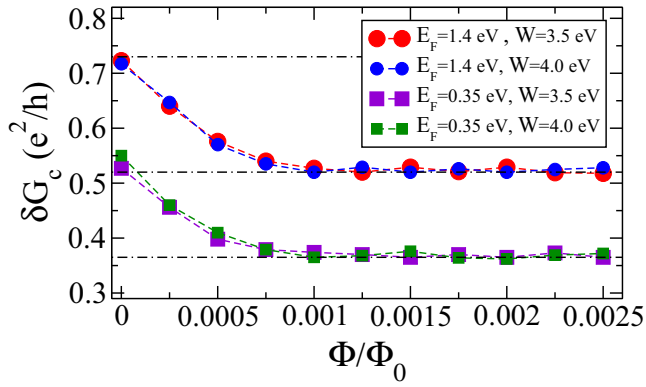

FIG. 7. The standard deviation of conductance δG_c of disordered z-GeSnH$_2$-NR with $N = 34$ and 51 nm length as a function of magnetic flux Φ/Φ_0.

The standard deviation of the conductance δG_c of the nanoribbon is also plotted as a function of disorder strength W at three different Fermi energies in Figs. 8(a)–8(c) for three cases of applied magnetic fields ($\Phi/\Phi_0 = 0$, 5×10^{-5}, and 25×10^{-4}). In the presence of very weak magnetic fields, $\Phi/\Phi_0 = 0$ to 5×10^{-5}, the UCF values remain unchanged. Therefore, the universality class for Fermi energies $E_F = 0.1$ eV and $E_F = 0.35$ eV [Figs. 8(a) and 8(b)] belong to the CUE ($\beta = 2$), while for high energies and strong disorder [Fig. 8(c)] the fluctuations follow the COE ($\beta = 1$). When $\Phi/\Phi_0 = 25 \times 10^{-4}$, which is greater than a certain threshold $\Phi/\Phi_0 = 10^{-3}$, the TRS is fully broken and the UCF value decreases by a factor of $\sqrt{2}$. For weak disorder in Fig. 8(a) the fluctuations are shown to be near zero due to the robustness of the edge states up to $\Phi/\Phi_0 = 25 \times 10^{-4}$ where the overlap of a pair of spin-polarized edge states gradually increases and this overlap develops fluctuations in the conductance. By applying large enough magnetic fields, the Kramer degeneracy is lifted and the two blocks of the Hamiltonian $H_\uparrow$ and $H_\downarrow$ contribute independently to δG_c, resulting in conductance fluctuations of $\delta G_c = 0.365$ as shown in Figs. 8(a) and 8(b). Note that in this situation the system belongs to the CUE and $\beta = 2$.

For high energies and strong disorder strengths, where SOC is negligible, the magnetic field breaks the TRS and changes the symmetry class of the system. As shown in Fig. 8(c) for $\Phi/\Phi_0 = 25 \times 10^{-4}$ the conductance fluctuations δG_c is around 0.52 indicating that the system belongs to CUE ($\beta = 2$).

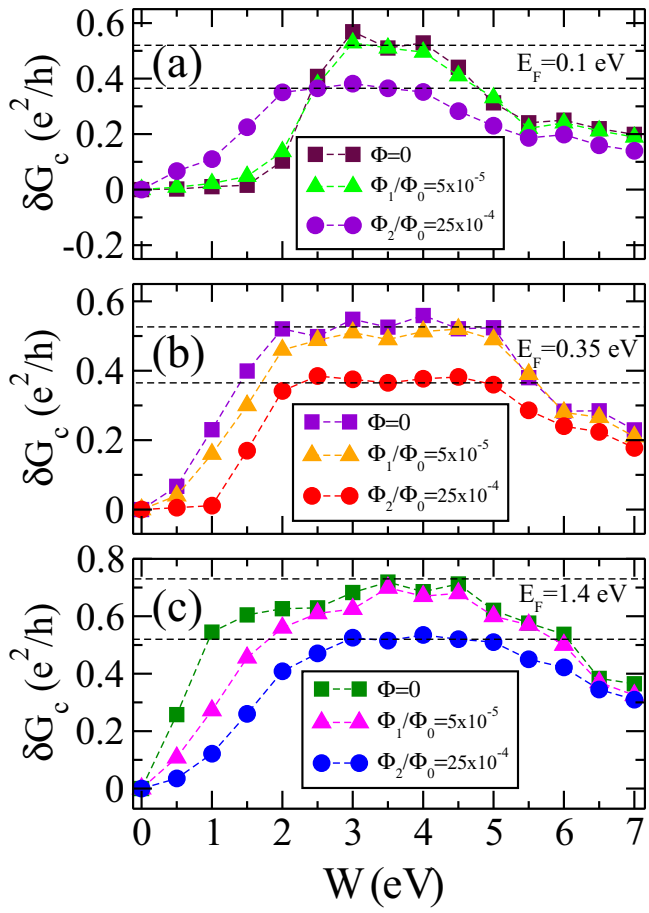

FIG. 8. The standard deviation of conductance δG_c of z-GeSnH$_2$-NR with $N = 34$ and 51 nm length as a function of disorder strength W for three different Fermi energies (a) $E_F = 0.1$ eV, (b) $E_F = 0.35$ eV, and (c) $E_F = 1.4$ eV.

VI. SUMMARY AND CONCLUSIONS

In summary, we constructed an effective TB model without and with SOC for ML GeSnH$_2$, which is able to reproduce the electronic spectrum in excellent agreement with the DFT results near the Fermi level. Including SOC decreases the band gap from 1.155 to 0.977 eV. In the presence of biaxial tensile strain, our proposed TB model predicts correctly the evolution of the band spectrum and also predicts a topological phase transition from NI to TI phase in ML GeSnH$_2$ at 7.5% biaxial tensile strain. The global bulk gap, which is topologically protected, is 134 meV at a reasonable strain of 8.5%. This bulk gap exceeds the thermal energy at room temperature and is large enough to make ML GeSnH$_2$ suitable for room-temperature spintronics applications.

The strong SOC and the applied mechanical strain are two essential factors that induce the topological phase transition from NI to QSH phase in ML GeSnH$_2$. More interestingly, ML GeSnH$_2$ is a strain-induced TI with inversion asymmetry which makes it a promising candidate for the understanding of intriguing topological phenomena like magnetoelectric effects. The TI nature of ML GeSnH$_2$ for strain $\epsilon > 7.5\%$ was confirmed by calculating the $\mathbb{Z}_2$ topological invariant. Also we showed the existence of topologically protected gapless edge states in a typical z-GeSnH$_2$-NR in the presence of biaxial strain $\epsilon > 7.5\%$.

An applied external magnetic field produces a QH phase in addition to the QSH phase. These two phases coexist up to a critical strength of the magnetic field at which the QSH phase completely disappears and the system becomes a pure QH insulator.

In addition we found topologically protected gapless edge states in a typical z-GeSnH$_2$-NR for a biaxial strain of $\epsilon = 8.5\%$ in the presence of disorder by calculating electronic transport. The conductance fluctuations reach the universal

TABLE II. The first column are the matrix elements for the nearest-neighbor hopping between s and the different p orbitals. The hopping integrals as a function of direction-dependent quantities and SK parameters are listed in the second column. The third column represents the hopping parameters with inclusion of applied strain.

Hopping parameters	Without strain	With biaxial strain
t_{ss}	$V_{ss\sigma}$	$t^0_{ss}[1-2\epsilon\cos^2\phi_0]$
t_{sp_x}	$lV_{sp\sigma}$	$t^0_{sp_x}[1-2\epsilon\cos^2\phi_0+\eta\epsilon\tan\phi_0]$
$\bar{t}_{sp_x}$	$l\overline{V}_{sp\sigma}$	$\bar{t}^0_{sp_x}[1-2\epsilon\cos^2\phi_0+\eta\epsilon\tan\phi_0]$
t_{sp_y}	$mV_{sp\sigma}$	$t^0_{sp_y}[1-2\epsilon\cos^2\phi_0+\eta\epsilon\tan\phi_0]$
$\bar{t}_{sp_y}$	$m\overline{V}_{sp\sigma}$	$\bar{t}^0_{sp_y}[1-2\epsilon\cos^2\phi_0+\eta\epsilon\tan\phi_0]$
$t_{p_xp_x}$	$l^2V_{pp\sigma}+(1-l^2)V_{pp\pi}$	$t^0_{p_xp_x}[1-2\epsilon\cos^2\phi_0+2\eta\epsilon\tan\phi_0]-2\eta\epsilon\tan\phi_0V_{pp\pi}$
$t_{p_yp_y}$	$m^2V_{pp\sigma}+(1-m^2)V_{pp\pi}$	$t^0_{p_yp_y}[1-2\epsilon\cos^2\phi_0+2\eta\epsilon\tan\phi_0]-2\eta\epsilon\tan\phi_0V_{pp\pi}$
$t_{p_xp_y}$	$lm(V_{pp\sigma}-V_{pp\pi})$	$t^0_{p_xp_y}[1-2\epsilon\cos^2\phi_0+2\eta\epsilon\tan\phi_0]$

value of the unitary class $\beta=2$. For high Fermi energies and strong disorder the conductance fluctuations follow the orthogonal ensemble $\beta=1$. The application of an external magnetic field gradually decreases the UCF by a factor of $\sqrt{2}$.

ACKNOWLEDGMENT

This work was supported by the FLAG-ERA project TRANS-2D-TMD.

APPENDIX: LOW-ENERGY EFFECTIVE TB HAMILTONIAN FOR MONOLAYER $GeSnH_2$

1. Tight-binding model Hamiltonian without SOC

To describe the low-energy spectrum and the electronic properties of ML $GeSnH_2$, we construct a TB model Hamiltonian involving the three outer shells s, p_x, and p_y atomic orbitals of Ge and Sn atoms. The effective TB Hamiltonian without SOC can be written in the second quantized representation as

$$H_0=\sum_{i,\alpha}E_{i\alpha}c^\dagger_{i\alpha}c_{i\alpha}+\sum_{\langle i,j\rangle;\alpha,\beta}t_{i\alpha,j\beta}(c^\dagger_{i\alpha}c_{j\beta}+\text{H.c.}). \tag{A1}$$

Here $\alpha,\beta\in(s,p_x,p_y)$ are the orbital indices and $\langle i,j\rangle$ denotes the nearest-neighboring ith and jth atoms. $E_{i\alpha}$ is the on-site energy of the αth orbital of the ith atom, $c^\dagger_{i\alpha}(c_{i\alpha})$ is the creation (annihilation) operator of an electron in the αth orbital of the ith atom, and $t_{i\alpha,j\beta}$ is the nearest-neighbor hopping parameter between the αth orbital of the ith atom and the βth orbital of the jth atom. The hopping parameters of Eq. (A1) are determined by the Slater-Koster (SK) [31] integrals as shown in the second column of Table II, where $l=\cos\theta\cos\phi_0$ and $m=\sin\theta\cos\phi_0$ are direction cosines of the angles of the vector connecting two nearest-neighboring atoms with respect to x and y axes, respectively.

We calculated the hopping parameters and on-site energies of the above Hamiltonian using the method of minimization of the least square difference between the DFT obtained band structure based on the Heyd-Scuseria-Ernzerhof (HSE) approximation [11] and the band structure of our TB model. Our TB model Hamiltonian has nine fitting parameters; namely, four on-site orbital energies ($E_{\mathrm{Ge},s}$, $E_{\mathrm{Ge},p}$, $E_{\mathrm{Sn},s}$, $E_{\mathrm{Sn},p}$) and five SK parameters related to the hopping energies ($V_{ss\sigma}$, $V_{sp\sigma}$, $\overline{V}_{sp\sigma}$, $V_{pp\sigma}$, $V_{pp\pi}$). Note that $V_{sp\sigma}$ ($\overline{V}_{sp\sigma}$) is the hopping integral between the s orbitals of atoms in sublattice A (B) and p orbitals of atoms in sublattice B (A).

Table III presents the obtained numerical values of the SK parameters. Using the optimized parameters, we can reproduce the three low-energy bands near the Fermi level (s and p_{xy} bands). Figure 9(a) shows the TB low-energy bands of ML $GeSnH_2$ that is in good agreement with the DFT results. The band structure has a direct band gap of 1.155 eV at the Γ point.

TABLE III. Numerical values of the SK parameters obtained from a fitting to the *ab initio* results. The energy units are eV.

$V_{ss\sigma}$	$V_{sp\sigma}$	$\overline{V}_{sp\sigma}$	$V_{pp\sigma}$	$V_{pp\pi}$	$E_{\mathrm{Ge},s}$	$E_{\mathrm{Ge},p}$	$E_{\mathrm{Sn},s}$	$E_{\mathrm{Sn},p}$
−1.51	3.33	2.35	3.69	−1.03	−5.47	5.23	−2.26	1.91

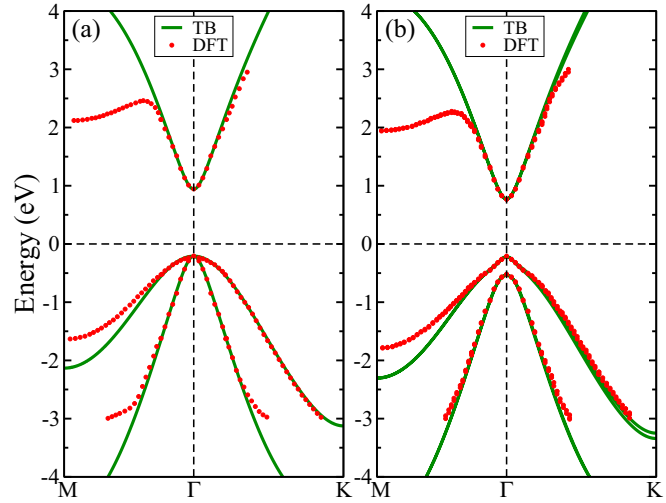

FIG. 9. The TB band structure of ML $GeSnH_2$ (a) without SOC and (b) with SOC. Symbols represent the DFT-HSE data taken from Ref. [11].

2. Spin-orbit coupling in ML $GeSnH_2$

In general, spin-orbit interaction can be written as [32]

$$H_{\mathrm{SOC}} = \frac{\hbar}{4m_0^2c^2}(\nabla V \times \boldsymbol{p})\cdot\boldsymbol{\sigma}, \tag{A2}$$

where $\hbar$ is Planks constant, m_0 is the rest mass of an electron, c is the velocity of light, V is the potential energy, $\boldsymbol{p}$ is momentum, and $\boldsymbol{\sigma}$ is the vector of Pauli matrices. The major part of SOC in systems that consist of heavy atoms comes from the orbital motion of electrons close to the atomic nuclei. In such systems and within the central field approximation, the crystal potential $V(\boldsymbol{r})$ can be considered as an effective spherical atomic potential $V_i(\boldsymbol{r})$ located at the ith atom. Therefore, by substituting $\nabla V_i(\boldsymbol{r}) = (dV_i/dr)\boldsymbol{r}/r$ and $\boldsymbol{s} = (\hbar/2)\boldsymbol{\sigma}$ terms into Eq. (A2) the SOC term takes the form [32]

$$H_{\mathrm{SOC}} = \lambda(r)\boldsymbol{L}\cdot\boldsymbol{s}. \tag{A3}$$

The above equation can also be expressed in the form

$$H_{\mathrm{SOC}} = \lambda(r)\left(\frac{L_+s_- + L_-s_+}{2} + L_zs_z\right), \tag{A4}$$

where $\lambda(r) = 1/2m_o^2c^2(1/r)(dV/dr)$ is the effective atomic SOC constant whose value depends on the specific atom. $L_\pm$, $s_\pm$ are the operators for angular momentum and spin, respectively. In the basis set of $|s_A, p_{xA}, p_{yA}, s_B, p_{xB}, p_{yB}\rangle \otimes |\uparrow,\downarrow\rangle$, the matrix elements of the on-site SOC Hamiltonian for ML $GeSnH_2$ are given by

$$\langle\alpha_i|H_{\mathrm{SOC}}|\beta_i\rangle = \lambda_i\left\langle\frac{L_+s_- + L_-s_+}{2} + L_zs_z\right\rangle_{\alpha\beta}. \tag{A5}$$

Here α_i and β_i are the atomic orbitals and λ_i is the on-site SOC strength of the ith atom. Note that since the two atoms in the unit cell of ML $GeSnH_2$ are different, we have two distinct SOC strengths λ_A and λ_B for atoms in sublattice A (Ge atoms) and sublattice B (Sn atoms), respectively.

The resulting SOC Hamiltonian matrix in the above basis is given by

$$H_{\mathrm{SOC}} = \begin{pmatrix} H_{\mathrm{SOC}}^{\uparrow\uparrow} & H_{\mathrm{SOC}}^{\uparrow\downarrow} \\ H_{\mathrm{SOC}}^{\downarrow\uparrow} & H_{\mathrm{SOC}}^{\downarrow\downarrow} \end{pmatrix}, \tag{A6}$$

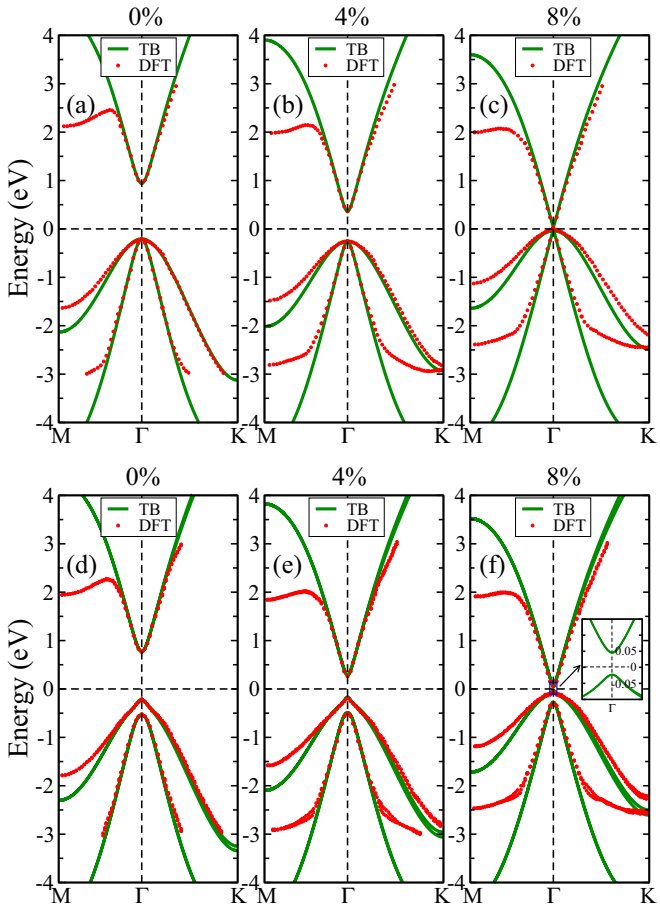

FIG. 10. The TB band structure of ML $GeSnH_2$ without (upper panels) and with (lower panels) SOC in the presence of (a) and (d) 0%, (b) and (e) 4%, and (c) and (f) 8% biaxial tensile strain. Red dots refer to the DFT-HSE data taken from Ref. [11].

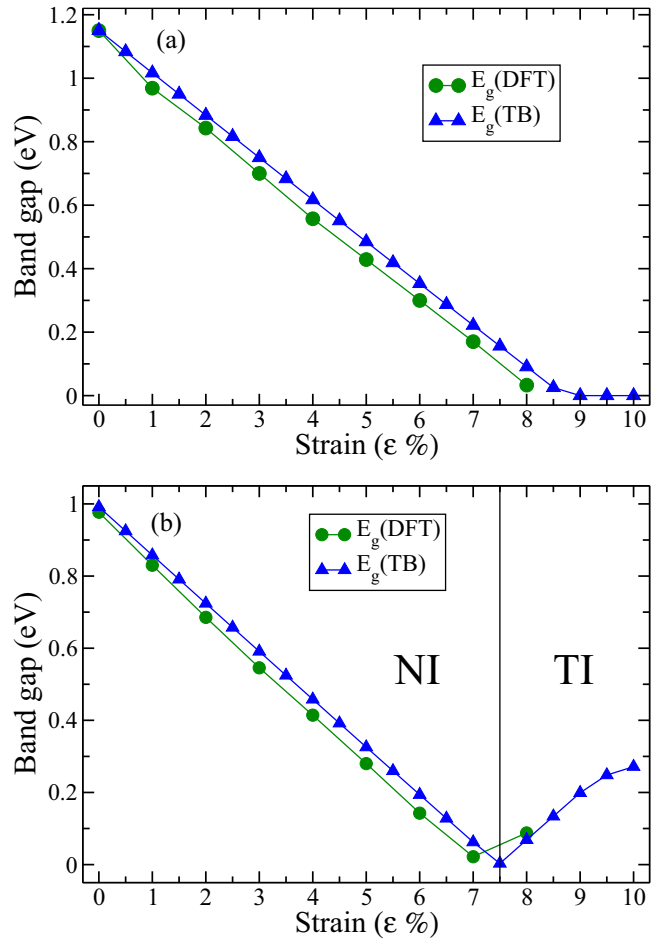

FIG. 11. The calculated band gaps of ML $GeSnH_2$ as a function of biaxial strain (a) without SOC, and (b) with SOC. The DFT data are taken from [11].

where the elements are 6×6 matrices

$$H_{\mathrm{SOC}}^{\uparrow\uparrow} = \frac{1}{2}\begin{pmatrix} 0 & 0 & 0 & 0 & 0 & 0 \\ 0 & 0 & -i\lambda_A & 0 & 0 & 0 \\ 0 & i\lambda_A & 0 & 0 & 0 & 0 \\ 0 & 0 & 0 & 0 & 0 & 0 \\ 0 & 0 & 0 & 0 & 0 & -i\lambda_B \\ 0 & 0 & 0 & 0 & i\lambda_B & 0 \end{pmatrix}, \quad \text{(A7)}$$

$$H_{\mathrm{SOC}}^{\downarrow\downarrow} = -H_{\mathrm{SOC}}^{\uparrow\uparrow}, \quad H_{\mathrm{SOC}}^{\uparrow\downarrow} = H_{\mathrm{SOC}}^{\downarrow\uparrow} = 0. \quad \text{(A8)}$$

The value of the on-site effective SOC strength λ is determined by fitting the TB energy bands to the DFT results. Here we fitted the energy bands obtained from our TB model to the one from the DFT+HSE approach [11]. The optimized numerical results using the hopping parameters from Table III are $\lambda_A = 0.296$ eV, $\lambda_B = 0.326$ eV for Ge and Sn atoms, respectively. The TB energy bands of ML $GeSnH_2$ in the presence of spin-orbit interaction using the mentioned values of SOC strengths are in good agreement with the *ab initio* results as shown in Fig. 9(b).

Notice from Fig. 9(b) the spin splitting in the doubly degenerate bands. The splitting is more clear for the upper valence band close to the K symmetry point which is 92 meV. For the conduction band the spin splitting is 241 meV at the K symmetry point. All the energy states of a system with inversion symmetry will be spin degenerate in case of TRS. The degeneracy can be lifted by breaking the inversion symmetry in such a system. The band gap of the system is reduced to 0.977 eV, demonstrating that ML $GeSnH_2$ is still a normal semiconductor.

3. The effect of strain

The electronic properties of a 2D system is affected significantly by applying strain [33,34]. This is due to the fact that strain changes both the bond lengths and the bond angles. This in turn changes the SK parameters and hopping integrals that further affect the electronic band structure.

Based on our knowledge from previous works, we expect a topological phase transition upon the application of biaxial tensile strain [11]. Furthermore, since the electronic band structure of this system under strain is available from *ab initio* calculations, the comparison of our TB band structure with DFT results will be another verification for the correctness of our TB model Hamiltonian. To this end, using the approach of Ref. [10] we obtain the effect of strain on the hopping parameters which we list in Table II. Note that $t^0_{i\alpha,j\beta}$ indicates the unstrained hopping parameters, ϵ is the strength of the applied biaxial strain, and ϕ_0 is the initial buckling angle.

The Hamiltonian for the strained system can be obtained by substituting the new hopping parameters (last column of Table II) in the original Hamiltonian Eq. (A1). The calculated TB energy spectrum of ML $GeSnH_2$ are shown in Figs. 10(a)–10(c) without SOC and Figs. 10(d)–10(f) with SOC in the presence of 0%, 4%, and 8% biaxial tensile strains. As shown, these results are in good agreement with the DFT calculations [11].

In Figs. 11(a) and 11(b) we show the variation of the energy gap of ML $GeSnH_2$ as a function of biaxial tensile strain without and with SOC, respectively. As shown in Fig. 11(b), with increasing biaxial tensile strain in the presence of SOC, the band gap decreases and eventually a band inversion occurs at the critical value of 7.5% strain. By increasing the strain the band gap reaches ~134 meV at a reasonable strain of 8.5%.

Remarkably, the value of the band gap is significantly larger than k_BT at room temperature (~25 meV), and therefore large enough to realize the QSH effect in ML $GeSnH_2$ even at room temperature. The excellent agreement between the results of our TB model and the DFT calculations in predicting the band inversion in this system upon biaxial tensile strain, implicitly confirms the validity of our proposed TB model.

[1] X.-L. Qi and S.-C. Zhang, Rev. Mod. Phys. **83**, 1057 (2011).
[2] M. Z. Hasan and C. L. Kane, Rev. Mod. Phys. **82**, 3045 (2010).
[3] J. E. Moore, Nature (London) **464**, 194 (2010).
[4] C. L. Kane and E. J. Mele, Phys. Rev. Lett. **95**, 226801 (2005).
[5] C. L. Kane and E. J. Mele, Phys. Rev. Lett. **95**, 146802 (2005).
[6] F.-C. Chuang, L.-Z. Yao, Z.-Q. Huang, Y.-T. Liu, C.-H. Hsu, T. Das, H. Lin, and A. Bansil, Nano Lett. **14**, 2505 (2014).
[7] H. Zhang, C.-X. Liu, X.-L. Qi, X. Dai, Z. Fang, and S.-C. Zhang, Nat. Phys. **5**, 438 (2009).
[8] M. König, S. Wiedmann, C. Brüne, A. Roth, H. Buhmann, L. W. Molenkamp, X.-L. Qi, and S.-C. Zhang, Science **318**, 766 (2007).
[9] I. Knez, R.-R. Du, and G. Sullivan, Phys. Rev. Lett. **107**, 136603 (2011).
[10] M. Rezaei, E. T. Sisakht, F. Fazileh, Z. Aslani, and F. M. Peeters, Phys. Rev. B **96**, 085441 (2017).
[11] Y. Ma, L. Kou, A. Du, and T. Heine, Nano Res. **8**, 3412 (2015).
[12] S.-J. Zhang, W.-X. Ji, C.-W. Zhang, S.-S. Li, P. Li, M.-J. Ren, and P.-J. Wang, RSC Adv. **6**, 79452 (2016).
[13] S.-S. Li, W.-X. Ji, C.-W. Zhang, P. Li, and P.-J. Wang, J. Mater. Chem. C **4**, 2243 (2016).
[14] C.-C. Liu, W. Feng, and Y. Yao, Phys. Rev. Lett. **107**, 076802 (2011).
[15] Y. Xu, B. Yan, H.-J. Zhang, J. Wang, G. Xu, P. Tang, W. Duan, and S.-C. Zhang, Phys. Rev. Lett. **111**, 136804 (2013).
[16] E. Taghizadeh Sisakht, F. Fazileh, M. H. Zare, M. Zarenia, and F. M. Peeters, Phys. Rev. B **94**, 085417 (2016).
[17] T. Fukui and Y. Hatsugai, J. Phys. Soc. Jpn. **76**, 053702 (2007).
[18] B. Scharf, A. Matos-Abiague, and J. Fabian, Phys. Rev. B **86**, 075418 (2012).
[19] S.-B. Zhang, Y.-Y. Zhang, and S.-Q. Shen, Phys. Rev. B **90**, 115305 (2014).
[20] S. Datta, *Electronic Transport in Mesoscopic Systems* (Cambridge University Press, Cambridge, UK, 1995).
[21] S. Datta, *Quantum Transport: Atom to Transistor* (Cambridge University Press, Cambridge, UK, 2005).
[22] G. M. Gusev, Z. D. Kvon, O. A. Shegai, N. N. Mikhailov, S. A. Dvoretsky, and J. C. Portal, Phys. Rev. B **84**, 121302 (2011).
[23] J. S. Van Dyke and D. K. Morr, Phys. Rev. B **95**, 045151 (2017).

[24] P. A. Lee and D. S. Fisher, Phys. Rev. Lett. **47**, 882 (1981).
[25] P. A. Lee and A. D. Stone, Phys. Rev. Lett. **55**, 1622 (1985).
[26] Y. Hu, H. Liu, H. Jiang, and X. C. Xie, Phys. Rev. B **96**, 134201 (2017).
[27] H.-C. Hsu, I. Kleftogiannis, G.-Y. Guo, and V. A. Gopar, J. Phys. Soc. Jpn. **87**, 034701 (2018).
[28] D.-H. Choe and K.-J. Chang, Sci. Rep. **5**, 10997 (2015).
[29] T. Kaneko, M. Koshino, and T. Ando, Phys. Rev. B **81**, 155310 (2010).
[30] Z. Qiao, Y. Xing, and J. Wang, Phys. Rev. B **81**, 085114 (2010).
[31] J. C. Slater and G. F. Koster, Phys. Rev. **94**, 1498 (1954).
[32] C.-C. Liu, H. Jiang, and Y. Yao, Phys. Rev. B **84**, 195430 (2011).
[33] G. Bir and G. Pikus, *Symmetry and Strain-induced Effects in Semiconductors* (Wiley, New York, 1974).
[34] Y. Sun, S. E. Thompson, and T. Nishida, *Strain Effect in Semiconductors* (Springer, New York, 2010).